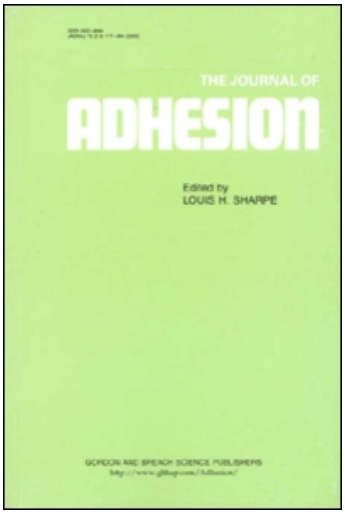

The Journal of Adhesion
Publication details, including instructions for authors and subscription information:
http://www.informaworld.com/smpp/title~content=t713453635

Fatigue Crack Growth in Structural Adhesives

D. A. Jablonski[a]
[a] United Technologies Research Center, East Hartford, CT, U.S.A.

To cite this Article Jablonski, D. A.(1980) 'Fatigue Crack Growth in Structural Adhesives', The Journal of Adhesion, 11: 2, 125 — 143
To link to this Article: DOI: 10.1080/00218468008078911
URL: http://dx.doi.org/10.1080/00218468008078911

J. Adhesion, 1980, Vol. 11, pp. 125–143
0021–8464/80/1102–0125 $06.50/0

Printed in Great Britain

Fatigue Crack Growth in Structural Adhesives

D. A. JABLONSKI
United Technologies Research Center, East Hartford, CT 06108, U.S.A.

(*Received February 13, 1980; in final form May 27, 1980*)

Fatigue crack growth rate studies of two high temperature structural adhesives, EA-9649 and AF-163, are described. It is shown that crack closure loads develop as a result of fatigue crack propagation. The fatigue crack propagation rates have been correlated with the strain energy release rate range, ΔG and with an effective strain energy release, ΔG_{eff}. The effective strain energy release rate range subtracts the strain energy due to crack closure from the applied strain energy release rate range.

The results show that there is a higher correlation between fatigue crack growth rate and ΔG_{eff} than between fatigue crack growth rate and ΔG. In EA-9649, 20 mil bond lines have higher fatigue crack growth rates than 10 mil bond lines at equal strain energy release rate ranges. The bond line thickness controls the closure load, with thicker bond lines having lower closure loads. By using ΔG_{eff} which accounts for crack closure, it is shown that fatigue crack growth rates are equivalent for 10 and 20 mil bond lines when compared at equal effective strain energy release rate ranges.

The fatigue fractures always followed a cohesive fracture path. In the scrim supported adhesive, two distinct fracture features were identified. Tear ridges were found adjacent to the scrim/adhesive interface, the tear ridges were formed by progressive debonding of the scrim from fatigue. Surface fatigue cracks were found on the scrim fibers which were caused by cyclic stressing of the scrim fibers from fatigue.

I. INTRODUCTION

Structural adhesives have become an accepted method of joining structural components together in such diverse fields as aircraft manufacture and sports equipment. Adhesive bonds have always suffered in the area of durability. The prediction of the strength and lifetime of adhesively bonded structures which contain flaws is a new technology area. Linear elastic fracture mechanics has been used to characterize the influence of flaws on the fatigue and fracture strengths of isotropic materials. The applicability of linear elastic fracture mechanics to adhesive bonds has been studied by

Presented at the Annual Meeting of the Adhesion Society, Savannah, GA, U.S.A., February 10–13, 1980.

Wang,[1] Trantina,[2] and Saxena.[3] They have shown that for center of bond cracking, linear elastic fracture mechanics can be used to characterize the crack tip stress field by use of either the stress intensity factor or the strain energy release rate. There is considerable disagreement as to how the stress intensity factor should be calculated, thus the strain energy release rate is the preferred parameter.

The strain energy release rate can be measured experimentally since it is related to the derivative of the compliance with respect to the crack length by the following equation:

$$G = \frac{P^2}{2b}\frac{\partial C}{\partial a}$$

By measuring the specimen compliance as a function of crack length, the strain energy release rate can be calculated. Mostovoy[4] has designed a contoured double cantilever beam specimen which maintains $\partial C/\partial a$ and, therefore, G independent upon crack length. This specimen has been used extensively in adhesive technology since the variation of bond properties with crack length can be studied at constant G.

There has been a limited number of investigations on fatigue crack propagation in adhesive bonds.[5–7] The fatigue crack growth rate has been correlated with the strain energy release rate range, ΔG. Mostovoy[5] and Marceau[6] found that the fatigue crack growth rate curve is sigmoidal in shape and that there is a threshold, ΔG_0, for propagating fatigue cracks. Temperature, humidity and test frequency have been shown to influence the fatigue crack growth rate.

One of the most controversial aspects of fatigue crack growth is the concept of crack closure which was first discovered by Elber.[8] Elber discovered that the crack remains closed during part of the fatigue loading cycle and it does not open until it reaches the "crack opening load" at which the crack tip first experiences the singularity of a theoretically sharp crack. The load at which the crack closes is called the "crack closure load" and is always greater than the crack opening load. Elber[8] attributes the closure phenomenon to the permanent tensile plastic deformations left in the wake of a propagating fatigue crack. Elber suggested that the closure effect is at least partially responsible for the interacting effects between stress levels under variable amplitude loading.

Since Elber's discovery of crack closure, there have been numerous investigations of crack closure in metallic alloys.[9–14] There have been many contradictory results on the effect of various variables on crack closure, but these studies have shown that crack closure is important to fatigue crack propagation. Studies by Lindley and Richards[12] have shown that crack closure loads are larger in plane stress regions than in plane strain regions. The larger closure loads in the surface plane stress region are

responsible for the curvature of the crack front.

Crack closure is a three dimensional phenomenon and must be measured by a technique which accounts for this. The best methods for measuring crack closure are electrical potential drop or compliance measurements with either a clip-on gage or strain gage. Optical measurements of crack closure, such as Elber's, are not as accurate since they only measure surface crack closure.

Fatigue crack closure has not been measured in adhesive bonds, but theoretically crack closure should occur, since plastic deformation will occur at the crack tip. Fatigue crack closure loads have been measured in this study by using aluminium contoured double cantilever beam specimens bonded with either EA-9649 or AF-163. The importance of fatigue crack closure to fatigue crack propagation is discussed.

II. EXPERIMENTAL PROCEDURES

Two high temperature structural adhesives, AF-163 and EA-9649, were used for this investigation. AF-163 manufactured by 3M Company, is a rubber filled, 250°F cure, film adhesive with a nylon scrim cloth support and EA-9649 manufactured by Hysol Company, is an aluminium, asbestos and rubber filled film adhesive with a 350°F cure. The adhesives were cured according to manufacturer's specifications with shims to control bond line thickness. Two plies of adhesive were used to make a 10 mil bond line and 4 plies of adhesive were used to make a 20 mil bond line.

Neat adhesive specimens were made by placing many plies of adhesive film in a rectangular mold and then curing the adhesive according to manufacturer's specification. The AF-163 neat adhesive specimen had nylon scrim cloth support and the EA-9649 neat adhesive specimen was unsupported.

Aluminium alloy 2024-T351 was used as the adherend. The surface preparation of the aluminium was done in five steps, which are: vapor degreasing, alkaline cleaning in a hot 5% NaOH solution, deionized water rinse, FPL etch, deionized water rinse. Immediately after the surface preparation, the adherends were spray primed with either BR-154 manufactured by Hysol Company, for EA-9649 bonding or EC-3924, manufactured by 3M Company, for AF-163 bonding. The primer thickness was between 0.20 and 0.50 mils.

The specimen design used for the fatigue crack propagation testing is shown in Figure 1. The contour $h = f(x)$ is set by the following equation:

$$4 = \frac{3x^2}{h^3} + \frac{1}{h} \tag{1}$$

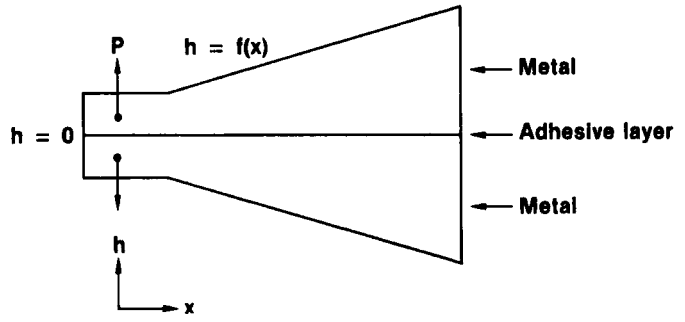

FIGURE 1 Schematic contoured double cantilever beam fatigue specimen.

The total length of the specimen was 6.75 inches and it was 0.500 inches thick. This specimen design maintains the strain energy release rate, G, independent of crack length by keeping the derivative of the compliance with respect to crack length, $\partial C/\partial a$, constant. The strain energy release rate is given by the following expressions:

$$G = \frac{P^2}{2b}\frac{\partial C}{\partial a} \tag{2}$$

$$\frac{\partial C}{\partial a} = \frac{8m}{Eb} \tag{3}$$

Experimental measurements of $\partial C/\partial a$ were made by extending a slot 0.006 inches in thickness in increments of 0.200 ± 0.002 inches and measuring the compliance at each slot length increment. This was used to obtain an accurate measurement of "m" and $\partial C/\partial a$. The experimental error in "m" and $\partial C/\partial a$ is approximately $\pm\frac{1}{2}\%$.

An MTS model 810 electrohydraulic testing system was used for the compliance measurements and fatigue testing. The fatigue specimens were cycled in load control using a sine wave at 40 Hz and a load ratio $R = 0.10$ ($R = P_{min}/P_{max}$). Crack length was measured optically by means of a traveling microscope and by compliance methods. The optical crack length measurement proved to be unreliable since the crack front bows and moves irregularly at the surface. The compliance method proved more reliable and was used as the accepted method crack length measurement.

The fatigue fractures were cut for scanning electron microscope analysis. Before examination, a thin layer of carbon was vacuum deposited on the fracture surface. A JEOL JSM-35 was used for the examination.

III. RESULTS AND DISCUSSION

The neat adhesive mechanical properties were measured at room temperature and the results are tabulated in Table I. The EA-9649 adhesive has a higher yield strength and modulus than AF-163 and it is also more brittle than AF-163. The EA-9649 is an aromatic novalac resin whereas the AF-163 is an aliphatic DEGBA type resin. The differences in chemistry are responsible for the higher strength and modulus of EA-9649 compared to AF-163.

TABLE I

Room temperature mechanical properties of AF-163, EA-9649 and 2024-T351 aluminium

Property	AF-163	EA-9649	2024-T351
Yield strength (psi)	5250.0	8440.0	47,000.0
Elastic modulus (psi $\times 10^6$)	0.34	0.78	10.6
Elongation (%)	2.42	1.75	20.0
Poisson's ratio	0.29	0.28	0.32

The specimen compliance as a function of crack length was measured on an aluminium specimen, for aluminium bonded with EA-9649 and for aluminium bonded with AF-163. The results are plotted in Figures 2–4. The compliance curve for the aluminium specimen had a linear relationship between compliance and crack length for cracks 1.50 to 3.75 inches in length. The nonlinear compliance at crack lengths greater than 3.75 inches is due to plastic deformation in the uncracked ligament. The slope of the curve and the "m" value agree within experimental error with the theoretical values of "m" and $\partial C/\partial a$.

$$m = 4.0 \text{ theoretical}$$

$$m = 3.96 \text{ experimental}$$

$$\partial C/\partial a = 6.05 \times 10^{-6} \text{ lb}^{-1} \text{ theoretical}$$

$$\partial C/\partial a = 5.97 \times 10^{-6} \text{ lb}^{-1} \text{ experimental}$$

The aluminium specimen bonded with 10 and 20 mil bond lines of EA-9649 had a linear relationship between compliance and crack length for cracks 1.50 to 3.75 inches in length. The deviation from linearity at crack lengths greater than 3.75 inches is due to plastic deformation in the uncracked adhesive layer. The bond line thickness does not change the compliance curves. The slope of the curve and the value of "m" are significantly reduced from that of the aluminium since the adhesives compliance is added to that of the

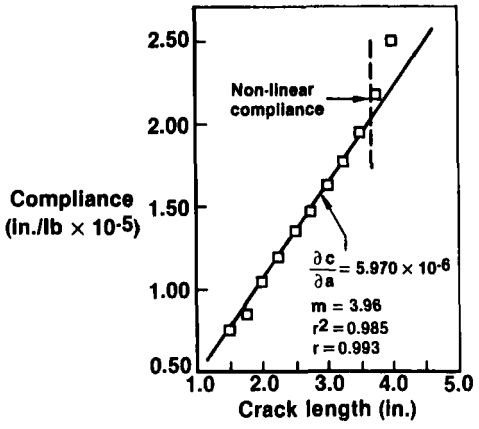

FIGURE 2 Compliance calibration curve of aluminium contoured double cantilever beam specimen.

metal. The value of $\partial C/\partial a$ from Figure 3 should be used in Eq. (2) to calculate the strain energy release rate for a specimen bonded with EA-9649.

The compliance curve for aluminium bonded with 10 and 20 mil bond lines of AF-163 is very similar to that of EA-9649. The differences between them are that the deviation from nonlinearity occurs at a shorter crack length, 3.25 inches compared to 3.75 inches, and the slope and "m" value are less for AF-163. The differences in the neat adhesive properties between EA-9649 and AF-163 can be used to explain the differences in their compliance curves. The lower yield strength of AF-163 is responsible for the shorter crack length for the nonlinear compliance deviation and its decreased modulus of elasticity is responsible for the lower value of $\partial C/\partial a$ for AF-163 compared to EA-9649.

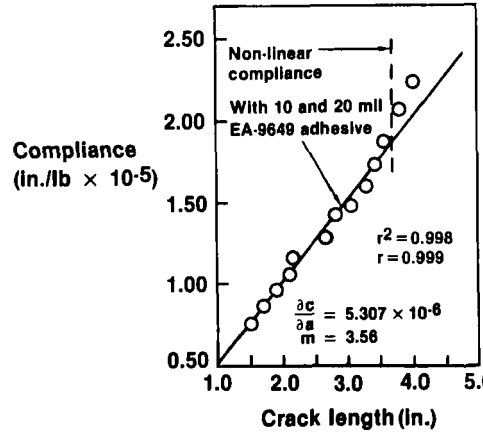

FIGURE 3 Compliance calibration curve of aluminium contoured double cantilever beam specimen bonded with EA-9649.

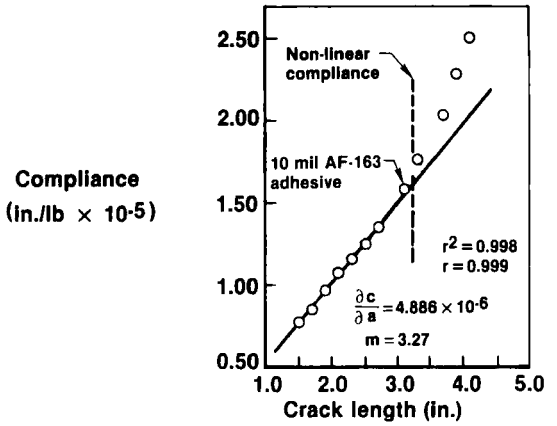

FIGURE 4 Compliance calibration curve of aluminium contoured double cantilever beam specimen bonded with AF-163.

The load deflection curves developed a nonlinear deflection at low loads during fatigue testing. The nonlinear deflection at low loads was due to fatigue crack closure. Fatigue crack closure occurs by the development of compressive stresses at the crack tip from fatigue cycling. Figure 5 shows a schematic illustration of the load deflection curves with and without crack closure. The closure load P_c is defined as the load at which the crack tip is at zero stress.

An accurate measurement of the closure load was made by strain gaging a fatigue specimen with three narrow strain gages (0.125×0.0625 inches), a technique first used by Paris and Schmidt[9] on aluminium compact tension specimens. Figure 6 shows the location of the three strain gages and the clip-on gage. The strain gage measurements can be converted to displacement measurements by multiplying the strain by the gage length (0.125 inches). The load displacement curves are shown in Figure 7 for an AF-163 specimen which was previously fatigue cycles at $\Delta G = 0.80$ lb/in for 100,000 cycles.

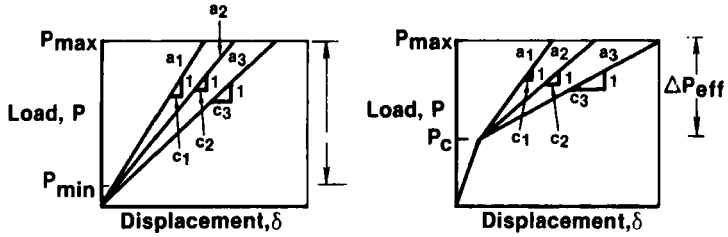

FIGURE 5 Schematic load displacement curves with and without crack closure.

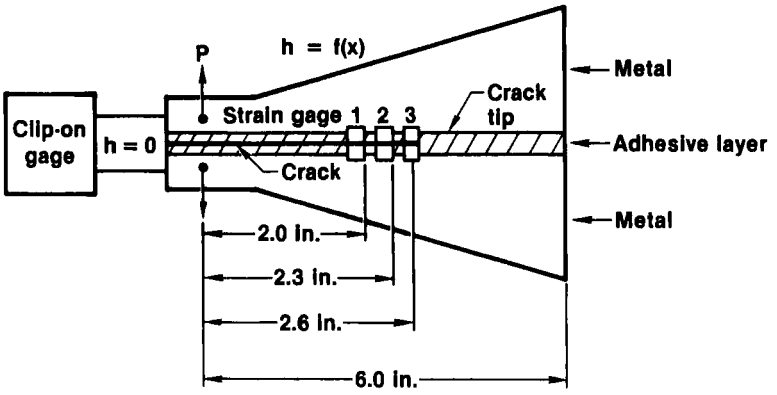

FIGURE 6 Placement of strain gages for crack closure measurements.

The strain gage measurements indicate that loading takes place in three stages; initially, the crack remains completely closed producing a linear record with no displacement. As the crack then begins to open, it produces a nonlinear load displacement record which finally becomes linear again when the crack is completely open. The load displacement curve for gage 3 does not represent the crack tip displacement since it was placed directly on the crack tip, but gages 1 and 2 do since they were placed far enough away from the crack tip. A comparison between the strain gage curves and the clip-on gage curve shows that the strain gages are more sensitive to crack closure than the clip-on gage.

The method used to determine closure load was different from that of

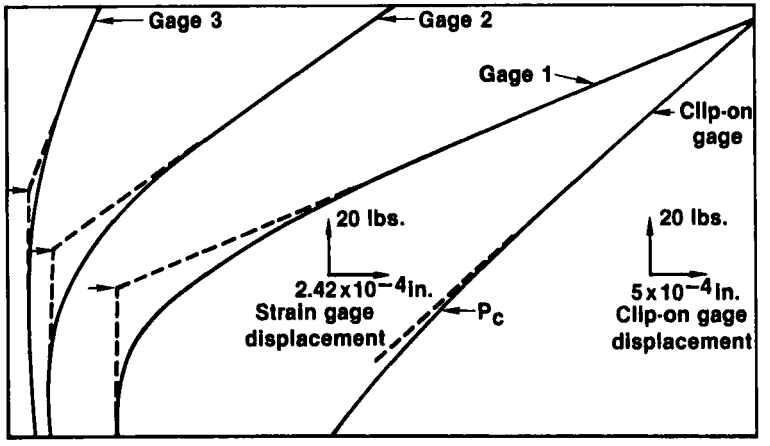

FIGURE 7 Fatigue crack closure measurements in AF-163 with a 10 mil bond line.

Paris and Schmidt. Tangents are drawn at the initial segment and final segment of the strain gage curves and the intersection of these two curves is defined as the closure load. A different definition of closure load was used for the clip-on gage curves since these curves are not linear at zero load. The closure load was defined at a 2×10^{-5} inches displacement deviation from nonlinearity from a tangent drawn from the upper segment of the curve. The measured closure loads are 46 lbs from the clip-on gage and 54 lbs from strain gage 1. The clip-on gage measurements were used to measure the crack closure load since this gage is not destroyed by fatigue cycling as the strain gages are. The numbers obtained by the two techniques are reasonably close.

Figure 8 is a plot of crack length versus cycles for EA-9649 with a 20 mil bond line. For each ΔG range a straight line was fitted to the data by a least squares method with the slope of the line representing the average fatigue crack growth rate. Figure 9 is a plot of crack length versus cycles for AF-163 with a 10 mil bond, with the slopes of the lines representing the average fatigue crack growth rates. In Figure 9, the data for two different specimens are plotted. There is a linear relationship between crack length and the number of cycles with both adhesives, which indicates that the crack growth rate is independent of crack length. The reasons for the independence is two-fold; the fatigue crack growth rate is controlled by both the driving force ΔG and material properties, and since neither of these variables vary with

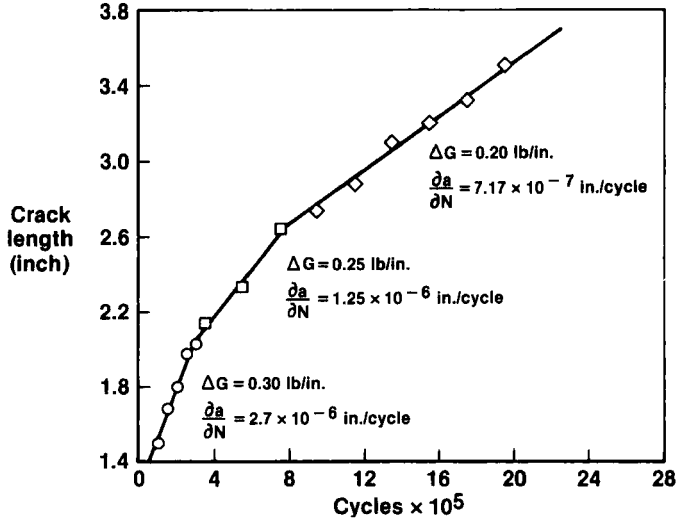

FIGURE 8 Crack length versus number of cycles for a contoured double cantilever beam specimen with a 20 mil EA-9649 bond line.

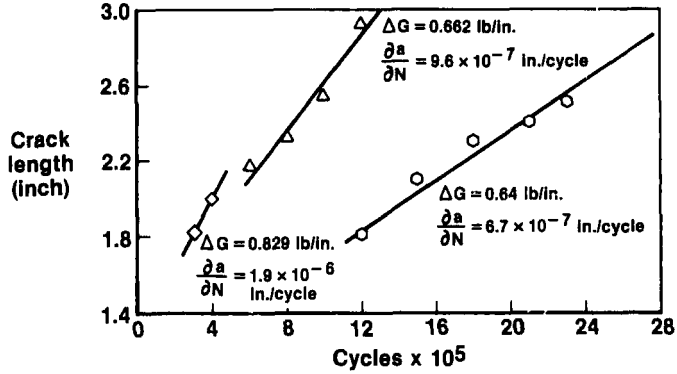

FIGURE 9 Crack length versus number of cycles for two contoured double cantilever beam specimens with a 10 mil AF-163 bond line.

crack length the average fatigue crack growth rate is independent of crack length.

The dependence of fatigue crack growth rate on the strain energy release rate range is shown in Figure 10 for aluminium bonded with EA-9649. The curve is sigmodal in shape with three different fatigue crack growth rate regions. The first region is identified by the threshold strain energy release rate and represents a ΔG value for non-propagating fatigue cracks. The threshold was defined as the ΔG value at which the crack growth rate was less than 10^{-8} in/cycle. To obtain the threshold ΔG_0, the strain energy release

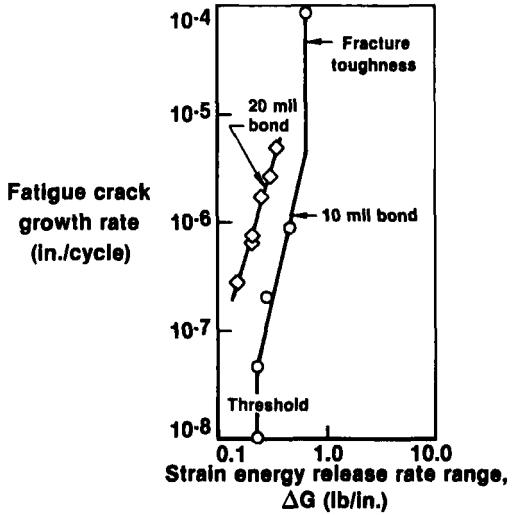

FIGURE 10 Fatigue crack growth rate versus ΔG for EA-9649 with 10 and 20 mil bond lines.

rate was reduced by 5% after each 0.050 inch length of crack propagation. This test procedure minimizes crack retardation due to the build up of compressive stresses from the previous ΔG range. The second region is the region in which there is a power law relationship between crack growth rate and ΔG.

$$\frac{da}{dN} = A\Delta G^n \tag{4}$$

For EA-9649 the exponent "n" was equal to 4.25. The third region of fatigue crack propagation is controlled by the fracture toughness G_{IC} and it represents the onset of catastrophic crack propagation.

The fatigue crack growth rate data shows that the bondline thickness influences the fatigue crack growth rate. The fatigue crack growth rates for the 20 mil bonds are an order of magnitude higher than those of the 10 mil bond samples. The threshold ΔG, though not measured for the 20 mil bond, will be lower than that of the 10 mil bond, since the data show that fatigue cracks propagate in the 20 mil bond line samples at ΔG's below the threshold of the 10 mil bond line samples.

The reason for the increased crack growth rate with the 20 mil bond line samples can be explained by crack closure. The crack closure loads for the 10 mil bond line samples are twice as large as they are for the 20 mil bond line samples (i.e., $\sim$80 lb versus $\sim$40 lb). The effective strain energy release rate range at the crack tip is less for the 10 mil bond line samples because of the higher closure load.

The effect of the closure load on the strain energy release rate can be calculated by substituting in an effective load range ΔP_{eff} in place of the applied load range ΔP. The equation for the strain energy release rate range can be simplified to the following expressions:

$$\Delta G = K\Delta P^2$$

defining

$$\Delta G_{\text{eff}} = K\Delta P_{\text{eff}}^2$$

where

$$\begin{aligned} \Delta P_{\text{eff}} &= P-(P_c-P_{\text{min}}) \quad \text{for } P_c > P_{\text{min}} \\ \Delta P_{\text{eff}} &= \Delta P \quad \text{for } P_c < P_{\text{min}} \end{aligned} \tag{5}$$

The closure load only influences the strain energy release rate when the closure load is greater than the minimum load in the cycle. The final equation for the effective strain energy release rate is:

$$\Delta G_{\text{eff}} = K(P_{\text{max}}-P_c)^2 \qquad P_c > P_{\text{min}} \tag{6}$$

$$\Delta G_{\text{eff}} = \Delta G \qquad P_c < P_{\text{min}} \tag{7}$$

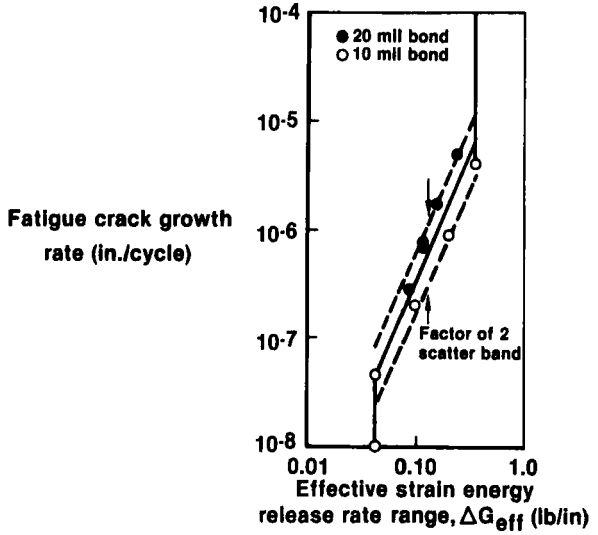

FIGURE 11 Fatigue crack growth rate versus ΔG_{eff} for EA-9649 with 10 and 20 mil bond lines.

The effective strain energy release rate range for EA-9649 was calculated from measured closure loads. The fatigue crack growth rate is plotted as a function of ΔG_{eff} for 10 and 20 mil bond lines in Figure 11. The data for 10 and 20 mil bond lines fall within a factor of two scatter band which is the

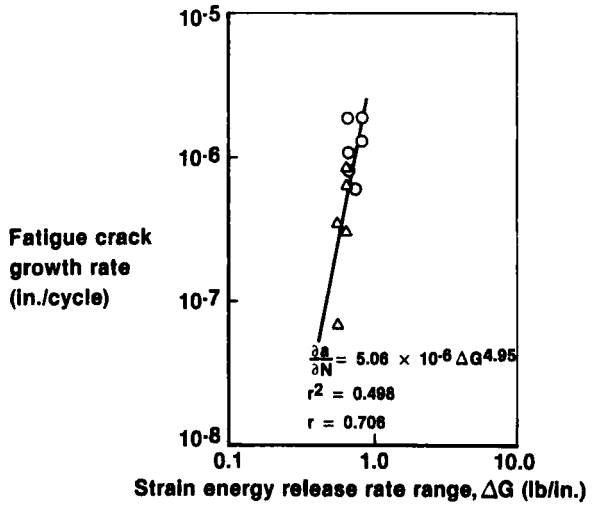

FIGURE 12 Fatigue crack growth rate versus ΔG for AF-163 with a 10 mil bond line.

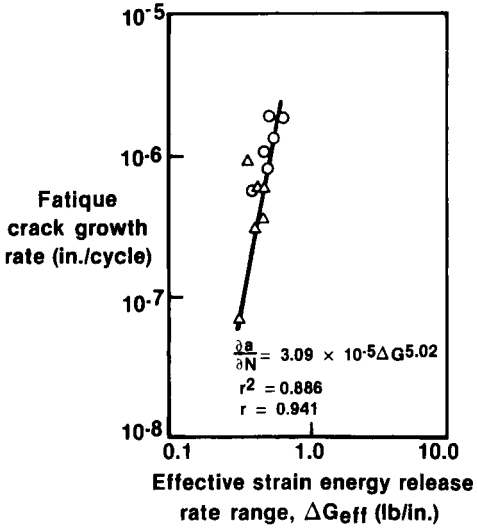

FIGURE 13 Fatigue crack growth rate versus ΔG_{eff} for AF-163 with a 10 mil bond line.

normal scatter for fatigue data. The data for 10 and 20 mil bond lines reresents the same data, therefore, there is no influence of bond line thickness on fatigue crack growth rate when the effective strain energy release rate is used.

The fatigue crack growth rate data for aluminium bonded with 10 mil AF-163 bond lines is shown in Figures 12 and 13 which are plots of fatigue crack growth rate as a function of ΔG and ΔG_{eff}. The lines drawn are least square fits of the data to Eq. 4 with "r" representing the coefficient of correlation. The correlation coefficient is much higher when ΔG_{eff} is used, (i.e., $r = 0.706$ for ΔG, $r = 0.941$ for ΔG_{eff}). The higher degree of correlation of fatigue crack growth rate with ΔG_{eff} proves that crack closure is a factor that influences fatigue crack growth substantially.

A study of the development of crack closure as a function of ΔG and the interactions involved going to and from different ΔG ranges were tested by use of a programmed load history fatigue test conducted on a bonded 10 mil AF-163 fatigue specimen. Figure 14 shows the variation of ΔG, da/dN and closure load with the number of cycles.

The test was concluded in four segments: first a crack was propagated 0.500 inches at $\Delta G = 0.60$ lb/in, then ΔG was increased to 0.80 lb/in and the crack was propagated an additional 0.500 inches, then ΔG was decreased to 0.60 lb/in and the crack was propagated an additional 0.500 inches and finally ΔG was decreased to 0.50 lb/in and the crack was propagated an additional 0.50 inches.

In the first two segments of the test, the closure load decreased with crack

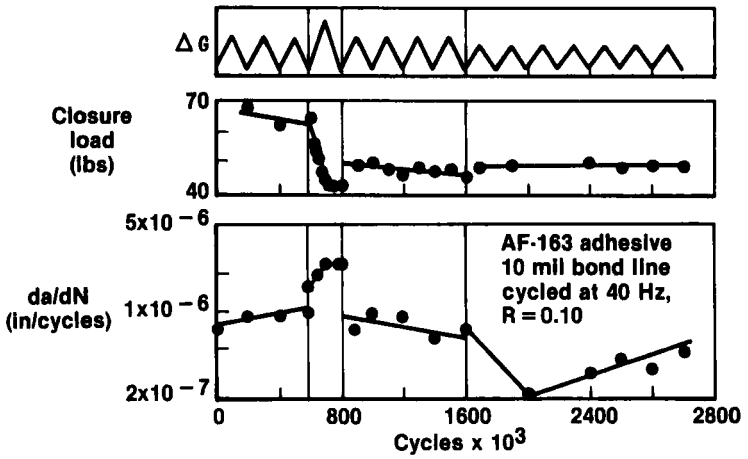

FIGURE 14 Fatigue crack growth rate and closure load versus the number of cycles for a programmed load history in AF-163 with a 10 mil bond line.

length and the crack growth rate increased with crack length, which is in accordance with an increasing ΔG_{eff} with decreasing closure load. In the second segment of the test where the closure load leveled off to ~40 lb and remained independent of the number of cycles, the fatigue crack growth rate also leveled off and remained independent of the number of cycles.

In the third segment of the test, the closure loads were constant and a slight decrease in fatigue crack growth rate was noted. In the last segment of the test, the closure load was independent of the number of cycles, but the fatigue crack growth rate initially decreased and then increased slowly with the number of cycles. The fatigue crack growth rate behavior in the final segment of the test cannot be explained by crack closure. This test proved that crack closure changes, with changes in load ranges, can explain some of the fatigue crack growth rate retardation behavior, but that the closure load cannot explain all of the retardation behavior in fatigue, due to changes in load ranges. This same conclusion has been made in a number of studies of metallic materials (see Ref. 10 and 11).

An important consideration in high frequency fatigue crack propagation testing is the temperature rise at the crack tip due to fatigue cycling. It is very difficult to measure this temperature rise, since it is confined to such a small area and the introduction of a probe to measure the temperature will disturb the stress distribution at the crack tip. The temperature rise can be calculated by using the analysis of Rice and Levey.[15] Their analysis considers a metallic system with a crack propagating at a velocity, V, under an applied stress intensity factor K_I. A conservative estimate of the temperature rise in an adhesively bonded structure can be obtained by replacing the metal

adherends by the adhesive. This approach will predict a higher temperature rise since it neglects the more rapid heat conduction in the metal adherends.

The temperature rise will be highest at the largest crack growth rate. For the EA-9649 adhesive, the thermal properties are:

$k = 5 \times 10^{-4}$ cal/cm-sec-C°	thermal conductivity
$C_p = 0.30$ cal/gm C°	specific heat
$\rho = 1.25$ gm/cm^3	density

The highest temperature rise occurs at a crack growth rate of 10^{-5} in/cycle and $\Delta G = 0.80$ lb/in. The other necessary properties are:

$V = 2.5 \times 10^{-4}$ in/sec	crack velocity
$K_I = 0.79$ ksi$\sqrt{\text{in}}$(i.e. $\sqrt{GE}$)	stress intensity factor
$\sigma_y = 8.4$ ksi	yield strength
$\nu = 0.28$	Poisson's ratio

The characteristic temperature for a running crack is u_c.[15] By using the values given above, u_c is calculated as 2.0°C. The temperature rise at the crack tip is equal to a quantity (u/u_c), which is a dimensionless quantity less than one, times u_c. The quantity, (u/u_c) is given by the solution of a Bessel function: its values is of order 10^{-2}. The temperature rise at the crack tip is of order 2×10^{-2}°C. The temperature rise at the crack tip is so small it can be neglected.

IV. FRACTOGRAPHY

All the fatigue fractures were cohesive with porosity observed on the fractures of both adhesives. In EA-9649 the fracture occurred close to the geometric center of the bond. In AF-163, the fracture initiated at the scrim cloth/adhesive interface. Scanning electron microscopy was used to identify fracture markings which would characterize the fracture as a fatigue fracture. In the AF-163 adhesive some distinct fracture features were seen because of the scrim cloth support in this adhesive. A few examples of these fracture markings are shown in Figures 15–17.

The fracture between the scrim cloth resembles a cleavage fracture, a typical example of this is shown in Figure 15. The cleavage fracture is due to the low ductility of the adhesive. Figure 16 shows debonding at the scrim adhesive interface. The debonding occurs progressively by fatigue cycling. Tear ridges are observed at the scrim/adhesive interface, parallel to the scrim fibers indicating that the debonding is progressive. Figure 17 shows fatigue cracks which form in the scrim cloth. The cracks are observed to occur primarily at bends in the scrim cloth. The cracks are only a few microns in depth and are formed when the scrim bridges the gap of the major crack

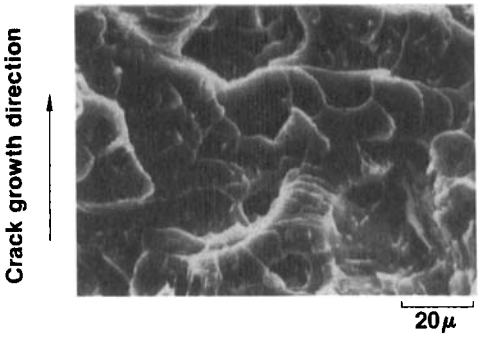

FIGURE 15 Fatigue fracture with a cleavage like appearance in between the scrim cloth in AF-163.

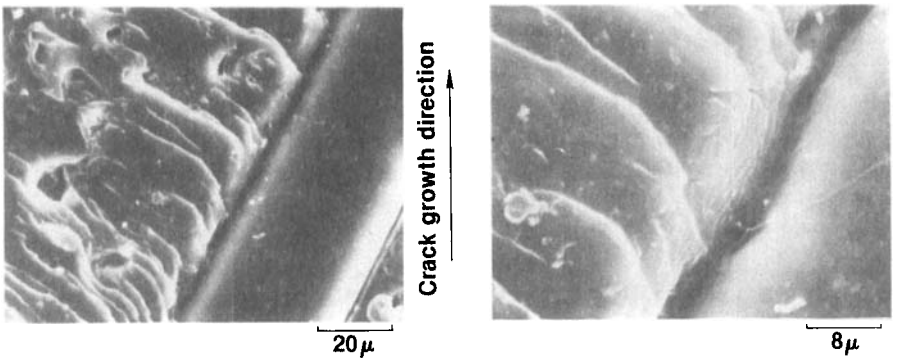

FIGURE 16 Tear ridges from progressive scrim debonding at the scrim/adhesive interface in AF-163.

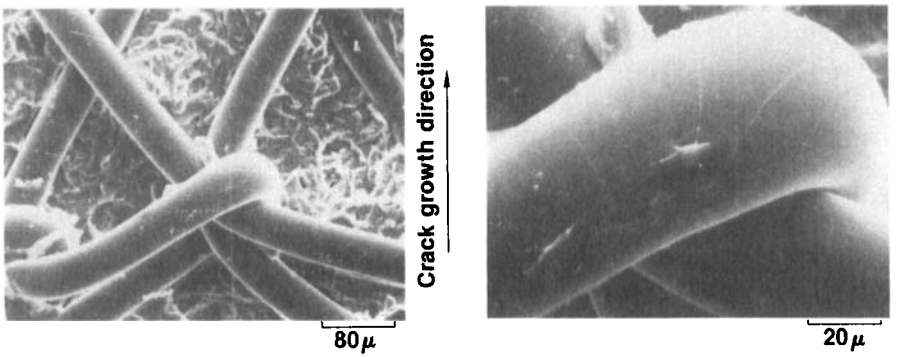

FIGURE 17 Surface fatigue cracks in the scrim cloth of AF-163.

front from each surface and is stressed mainly in bending from the fatigue cycling.

The occurrence of surface fatigue cracks in the scrim cloth is an observation which has not been previously reported before in the literature. These crack-like features were examined carefully before they were labeled as cracks. Examination of these crack-like features at 25,000× in the SEM using both the secondary electron image and the *y*-modulation image, which maps surface contour, showed that these features were indeed cracks. To avoid the possibility that the cracks were in the scrim cloth before fatigue cycling, the fast fracture or overload area was examined carefully for cracking in the scrim cloth. Cracking in the scrim cloth in this area was not found.

The proposed mechanism for the formation of these cracks is not related to the intersection of the main crack front with the scrim cloth, rather it deals with the stresses applied to the scrim fibers when the scrim fibers are attached to both fracture surfaces after the main crack front passes. After the main crack front passes, the scrim fibers which are still attached to both fracture surfaces will be subjected to cyclic tension and cyclic torsional stresses from the fatigue cycling. The cyclic tension stresses will cause circumferential cracking. The combination of cyclic tension and torsion will cause the cracks to form at 45° to 90° from the fiber axis. Figure 17 shows that the majority of the cracking in the scrim fibers is oriented between 45° and 90° from the fiber axis.

The SEM analysis has shown that in a scrim supported adhesive (AF-163) there are two characteristic fatigue fracture features. They are tear ridges at the scrim/adhesive interface and surface cracking in the scrim. In the unsupported adhesive (EA-9649) no distinct fatigue fracture features were found.

V. CONCLUSIONS

The following conclusions can be drawn from the results of this study:

- Fatigue crack closure occurs in adhesively bonded structures.
- The closure load increases with decreasing bond line thickness.
- Fatigue crack growth rate can be correlated with ΔG.
- A higher correlation can be obtained between fatigue crack growth rate and ΔG_{eff} than with ΔG.
- In EA-9649, 20 mil bond lines have higher fatigue crack growth rates when ΔG is used. When ΔG_{eff} is used, there is no influence of bond line thickness on fatigue crack growth rate.

- In scrim supported adhesives two characteristic fatigue fracture features are tear ridges at the scrim/adhesive interface and surface cracks in the scrim cloth.

Acknowledgements

The author would like to acknowledge the financial support of Pratt and Whitney Aircraft, JT-8D projects group, and, in particular, to Mr. Edgar McCulloch for program support. The author would also like to acknowledge Dr. Roscoe Pike for the many helpful discussions and Mr. Robert Girouard and Mr. Steven Sargent for technical assistance.

References

1. S. S. Wang, J. F. Mandell and F. J. McGarry, *International J. of Fracture* **14,** 38–59 (1978).
2. G. G. Trantina, *J. Composite Materials* **6,** 192–207 (1972).
3. A. Saxena, *Fibre Science and Technology* **12,** 111–128 (1979).
4. S. Mostovoy, P. B. Crosely and E. J. Ripling, *J. of Materials* **2,** 661–681 (1967).
5. S. Mostovoy and E. J. Ripling, *Adhesion Science and Technology Vol 9B* (Plenum Press, N.Y. 1975), pp. 513–562.
6. J. A. Marceau, J. C. McMillan and W. M. Scardino, Diversity Technology Explosion, SAMPE 22nd National SAMPE Symposium and Exhibition, 1977, Vol. 22, pp. 64–80.
7. T. R. Brussat, S. T. Chiu and S. Mostovoy, "Fracture Mechanics for Structural Adhesives"—Final Report, October 1977, AFML-TR-77-163.
8. W. Elber, *Engineering Fracture Mechanics* **2,** 37–45 (1970).
9. P. C. Paris and R. A. Schmidt, Progress in Flaw Growth and Fracture Toughness Testing, ASTM STP 536 (ASTM, Philadelphia, 1973), pp. 79–94).
10. S. Matsuoka, K. Tanaka and M. Kawahara, *Engineering Fracture Mechanics* **8,** 507–523 (1976).
11. D. Macha, *Engineering Fracture Mechanics* **12,** 1–11 (1979).
12. F. Lindley and C. Richards, *Materials Science and Engineering* **14,** 281–293 (1974).
13. A. McEvily, *Metal Science* **819,** 274–284 (1977).
14. P. Paris and L. Herman, Int. Cong. Appl. Mech., Delft, 1973.
15. J. R. Rice and N. Levey, in *Physics of Strength and Plasticity*, A. S. Argon, ed. (The M.I.T. Press, Cambridge, MA, 1969), pp. 277–293.

List of symbols

a = crack length
b = specimen thickness
h = specimen height
C = compliance
$\partial C/\partial a$ = derivative of compliance with respect to crack length
m = shape factor of contoured double cantilever beam specimen
P = applied load
P_{min} = minimum load
P_{max} = maximum load
ΔP = load range ($\Delta P = P_{max} - P_{min}$)

R = load ratio (P_{min}/P_{max})
P_c = closure load
ΔP_{eff} = effective load range
G = strain energy release rate
ΔG = strain energy release rate range
ΔG_{eff} = effective strain energy release rate range
ΔG_0 = threshold strain energy release rate range
N = number of cycles
da/dN = fatigue crack growth rate
K = constant for ΔG calculation
n = fatigue crack growth rate exponent
A = coefficient of fatigue crack growth rate relationship
k = thermal conductivity
Cp = specific heat
ρ = density
V = velocity
v = Poisson's ratio
u = temperature rise at crack tip
u_c = characteristic temperature for a propagating crack
K_I = stress intensity factor